JMEPEG (2008) 17:80–84
DOI: 10.1007/s11665-007-9116-1

1059-9495/$19.00

J-Q Characterization of Constraint Effects of a Three-Dimensional Cracked Specimen

Fernando Labbé and Juan R. Donoso

(Submitted January 10, 2007; in revised form February 21, 2007)

Failure assessment of the integrity of a ductile flawed structural component is done currently by a one-parameter fracture mechanics approach. The *J*-integral is the one-parameter used; it has proven to be useful in order to predict ductile crack initiation. However, when tension loading dominates and/or a fully plastic condition develops around the crack, the *J*-integral alone does not describe completely the crack-tip stress field and a second parameter is needed. In this work, an accurate modeling of the elastic-plastic stress field around a deep crack in a three-dimensional three-point bend specimen is carried out. Numerical results for the crack-tip stress field are used to evaluate a crack-tip constraint parameter *Q*, in terms of applied loading, from contained plasticity to large-scale yielding. The parameter *Q*, measures the degree of stress triaxiality and constraint around the crack-tip. In order to obtain the stresses in the near-crack-tip field with high accuracy, a detailed mesh with higher order three-dimensional finite elements is located around the crack front. The modeling of crack-tip blunting deformation is performed by using a small notch radius in the crack-tip. Large-strain and finite-rotation nonlinear behavior effects around the crack-tip are included. The material, an ASTM A 516 steel, is modeled with incremental theory of plasticity. Numerical results of the *Q* triaxiality parameter are presented for increasing level loads to obtain an extended yield condition. Additional results of *J*-integral parameter and crack-tip opening displacement, for different load ratios and for different position across the specimen thickness are shown.

Keywords constraint effects, finite element analysis, fracture mechanics

1. Introduction

Failure assessment of the integrity of a flawed structure has been based on the dominance of asymptotically singular crack-tip field, characterized by a single parameter, such as the *J*-integral. The singular crack-tip solution for a nonlinear material, obtained by Hutchinson (Ref 1) and Rice and Rosengren (Ref 2), is referred as the HRR singularity field. The *J*-integral parameter measures the intensity of the crack-tip stress/deformation fields around the crack-tip and has been proven by Begley and Landes (Ref 3) to be a viable parameter for predicting ductile crack initiation and growth under monotonic loading. There is general agreement that the applicability of this one-parameter approach is limited to a high crack-tip constraint, which is often related to high stress triaxiality at the crack-tip. Hence, the region around the crack can be adequately described by the HRR singularity field for loads ranging from small-scale yielding to moderate large-scale plasticity (Ref 4).

However, for specimens with a low crack-tip constraint, the dominance of single-parameter based singular fields exists only at small plasticity. At large plasticity, the crack-tip triaxiality of low-constraint specimens is lower than the predicted by the single-parameter based singular fields. Consequently, such specimens often exhibit higher fracture toughness than high-constraint specimens if the fracture process occurs after large plastic deformation. This behavior, referred to as constraint effects in fracture, is evidenced by a tendency for a given material to show variations in the value of *J* at the onset of fracture as the specimen geometry and loading configuration are changed (Ref 5).

ASTM E-1820-99 (Ref 6) standards for fracture toughness evaluation of J_{IC} require sufficient specimen thickness to produce predominantly plane strain conditions at the crack-tip. These restrictions are designed to insure the existence of severe conditions for fracture as described by the HRR asymptotic fields. However, many important flawed structures show a low crack-tip constraint, which leads to a very conservative prediction of structural integrity based on laboratory fracture toughness values. Consequentially, modern approaches in fracture mechanics are aimed to consider that constraint of the fracture test specimen approximates that of the structure to provide a more realistic toughness for use in the assessment of structural integrity.

In the last few years, considerable efforts have been made to analyze the effect of constraint in fracture (Ref 7). Some important contributions have been done by O'Dowd and Shih (Ref 8, 9), Betegon and Hancock (Ref 10), Hancock et al. (Ref 11), Dodds et al. (Ref 12), and Wang and Parks (Ref 13). In the O'Dowd and Shih (Ref 8, 9) approach, a second parameter *Q* is used to measures the degree of triaxiality and constraint of the crack-tip stress field. Hence, the *J-Q* methodology gives a characterization of the crack-tip field stress-field, with a *Q* parameter, which determines the crack-tip stress triaxiality and

Fernando Labbé and **Juan R. Donoso,** Universidad Técnica Federico Santa María, Avenida España 1680, Valparaíso, Chile. Contact e-mail: fernando.labbe@usm.cl.

a J-parameter setting the stress level and the size scale over which large stresses and strains develop.

Constraint effects in fracture are closely related to the crack-tip behavior, which is complex due to several reasons. The fracture process zone occurs very close to the crack-tip where finite strain and high gradient stress/strain exist. In addition, a finite deformation blunting of the crack-tip exists and hence, small strain theory does not model blunting correctly. Strain gradients that develop around a crack front cause deformation in the local region to be constrained by the surrounding material. The level of constraint depends upon the crack configuration and crack location relative to external boundaries. Finally, constraint effects produce a three-dimensional crack-tip stress field, which differs from those in plane strain and plane stress, and strongly influence fracture behavior. Therefore, for a clearly understanding of the three-dimensional crack-tip field behavior, a full and detailed three-dimensional finite element analysis needs to be done.

This paper presents a detailed three-dimensional finite element analysis for the elastic-plastic stress field around a deep crack in a three-point bend specimen. Numerical results are used to evaluate the evolution of the constraint Q parameter, for a loading situation ranging from small- to large-scale yielding. An accurate modeling of crack-tip blunting deformation was done by using a small notch radius in the crack-tip. Large-strain and finite-rotation effects around the crack-tip were included. The material, an A-516 steel Gr. 70, is modeled with incremental theory of plasticity. Additional results of J-integral parameter and crack-tip opening displacement (CTOD) in terms of load ratios are presented for different position across the thickness.

2. *J-Q* Description of Crack-Tip Stress Field

The general elastic-plastic behavior of hardening material described by the Ramberg-Osgood power-law stress-strain relation can be written as

$$\frac{\varepsilon}{\varepsilon_0} = \alpha\left(\frac{\sigma}{\sigma_0}\right)^n \quad \text{(Eq 1)}$$

where n is the strain hardening exponent, α is a material constant, σ_0 is the yield stress, and ε_0 is the yield strain given by σ_0/E, with E the Young's modulus.

Based on asymptotic and finite element results, for distances sufficiently close to the crack-tip but still outside of the zone of finite strain, O'Dowd and Shih (Ref 8, 9) proposed the following representation for the plane strain crack-tip stresses:

$$\frac{\sigma_{ij}}{\sigma_0} = \left[\frac{J}{\alpha\sigma_0\varepsilon_0 I_n r}\right]^{1/n+1}\phi_{ij}(\theta,n) + Q\left[\frac{r}{J/\sigma_0}\right]^q \psi_{ij}(\theta,n) \quad \text{(Eq 2)}$$

where r and θ are the local cylindrical coordinates centered at the crack-tip. The normalizing factor I_n and the angular distribution of the dimensionless constants $\phi_{ij}(\theta,n)$ and $\psi_{ij}(\theta,n)$ are functions of the strain-hardening exponent n. The first term in the above expansion correspond to the HRR field, after Hutchinson (Ref 1) and Rice and Rosengren (Ref 2), with the J-integral parameter as amplitude. The dimensionless parameter Q measures the amplitude of the second term.

Further numerical results of O'Dowd and Shih (Ref 8, 9) show that the second term is essentially independent of the radial distance, $|q| \ll 1$, and the corresponding $\psi_{ij}(\theta,n)$ functions do not depend on θ. This means that the second term of the above expansion acts like a uniform hydrostatic stress in the sector. Hence, relation (2) may be written as

$$\frac{\sigma_{ij}}{\sigma_0} = \frac{(\sigma_{ij})_{HRR}}{\sigma_0} + Q\cdot\delta_{ij} \quad \text{(Eq 3)}$$

where $(\sigma_{ij})_{HRR}$ is the HRR asymptotic stress field and Q represents a triaxiality parameter. A negative Q means that the hydrostatic stress is reduced (low stress constraint) in comparison with the reference state (HRR field), and therefore the J one-parameter approach is no longer valid. On the other hand, structures with $Q \geq 0$ exhibit high stress triaxiality, good agreement with the HRR fields, and are, consequently, highly constrained components.

From Eq (3), Q may be evaluated as the difference between the actual full-stress field, and the HRR field as follows:

$$Q = \frac{(\sigma_{\theta\theta})_{FEM} - (\sigma_{\theta\theta})_{HRR}}{\sigma_0} \quad \text{(Eq 4)}$$

for $\theta = 0$ and normalized distance $r = 2J/\sigma_0$.

3. Finite Element Modeling of Three-Point Bend Specimen

The three-point bend specimen with a deep crack ($a/W = 0.7$) shown in Fig. 1 was modeled using three-dimensional finite elements. Geometric dimensions of the specimen are $L = 102$ mm (4″), $W = L/4$, thickness $B = 3.175$ mm (1/8″), and crack to wide ratio $a/W = 0.7$. Due to load and geometry symmetry, only one quarter of the specimen need to be considered, with appropriate boundary conditions imposed on the planes of symmetry. The in-plane mesh geometry for the quarter of specimen is shown in Fig. 2. The mesh consists of six layers of elements through half the plate thickness B. The in-plane mesh near the crack-tip is shown in Fig. 3, 4. The crack-tip blunting deformation was simulated by a small notch radius at the crack-tip. A notch radius of $a/1400$ was chosen, with a as the crack length. The in-plane dimension of the smallest element near the notch tip is $a/8400$. Finite strain plasticity and large rotation effects around the crack-tip were accounted for in the finite element model.

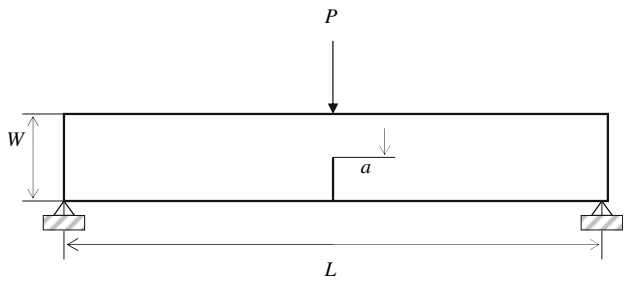

Fig. 1 The three-point bend specimen with a deep crack ($a/W = 0.7$). Geometric dimensions of the specimen are $L = 102$ mm (4″), $W = L/4$, and thickness $B = 3.175$ mm (1/8″)

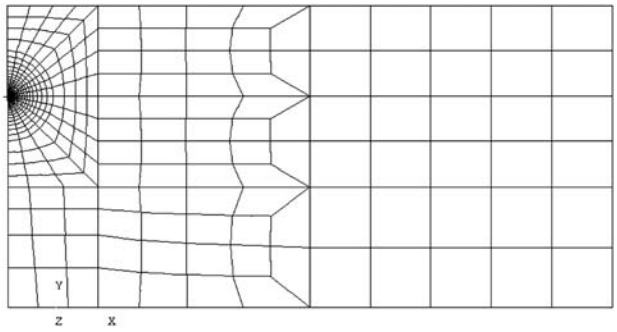

Fig. 2 Finite element mesh for the half specimen

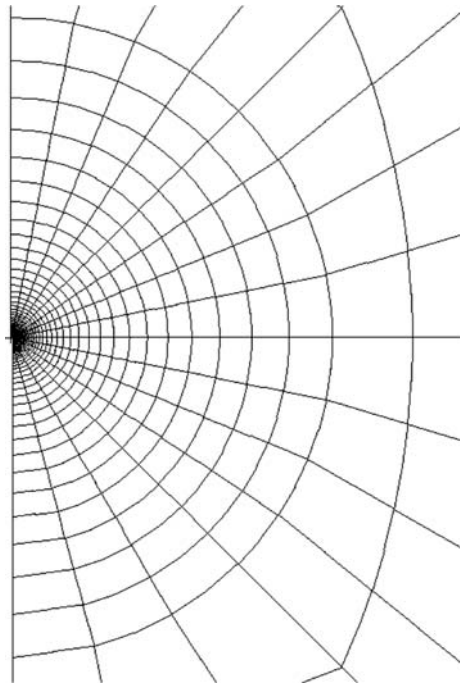

Fig. 3 Finite element mesh around the crack-tip

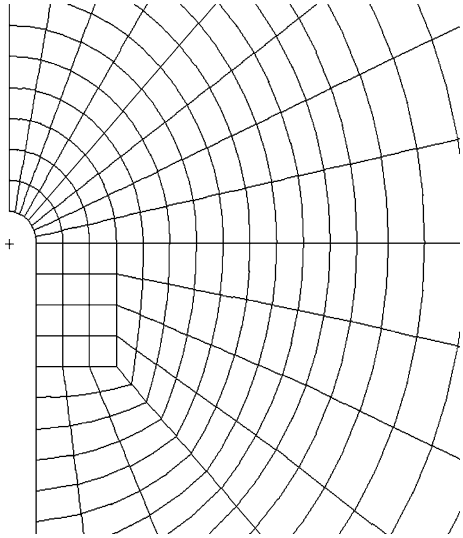

Fig. 4 Detail of the finite element mesh at the crack-tip blunting

The finite element code *Abaqus* was used in the analysis of the quarter specimen using a total number of 4212 high-order twenty-node, isoparametric elements. Reduced integration ($2\times2\times2$) is used to eliminate artificial locking under incompressible plastic deformation conditions.

The plastic behavior of the A 516 Gr. 70 steel was modeled using incremental theory with a von Mises yield surface, associate flow rule, and isotropic hardening. The yield stress is σ_0 = 360 MPa, and the Ramberg-Osgood material parameters are n = 4, and α = 1.

The J-integral around the crack at each load step was calculated by the domain integral method as is implemented in *Abaqus*. The J-values used were obtained as an average of J from 10 trajectory evaluations around the crack. Crack-tip opening displacement was obtained from displacements of nodes at the 90° intercept from the crack-tip, according to the procedure introduced by Shih (Ref 14).

4. Numerical Results

The variation of load versus load point displacement is shown in Fig. 5. The variation of J versus the applied load is shown in Fig. 6.

In Fig. 7, J normalized by J_0, evaluated at the center plane, is plotted against normalized distance, B/t, along the crack front for different ratios of the applied load P/P_0 (P_0 is the plane stress limit load and it is equal to 700 N). It is seen that with increasing plastic deformation, there is a considerable variation of J through the thickness with the value at the center being much higher than that at the free surface.

The CTOD at the half thickness plane of the three-dimensional specimen is plotted against the load in Fig. 8.

The variation of the CTOD, along the crack front is shown in Fig. 9 for three different load ratios P/P_0. As in the case of J in Fig. 7, there is a marked variation of the CTOD as plastic deformation increases, the value at the centerline being larger than with those at the free surface. This high variation of crack-tip opening through the thickness is coincident with experimental evidence in which the crack begins to propagate first at the center of the specimen (tunneling mode of fracture).

The stress component σ_{xx} normalized by the yield stress σ_0 versus tip normalized crack-tip distance $x/J/\sigma_0$ is shown in

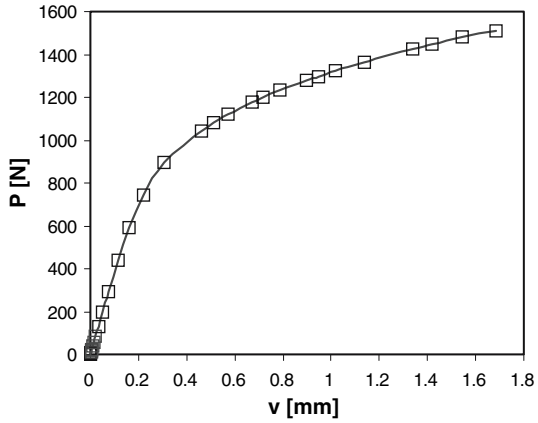

Fig. 5 Load versus load point displacement

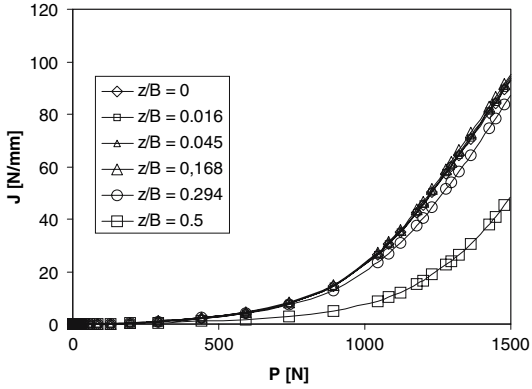

Fig. 6 *J*-values versus applied load

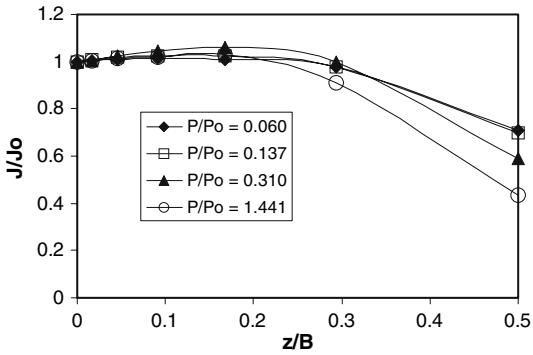

Fig. 7 Normalized *J*-values versus normalized distance *z*/*t*

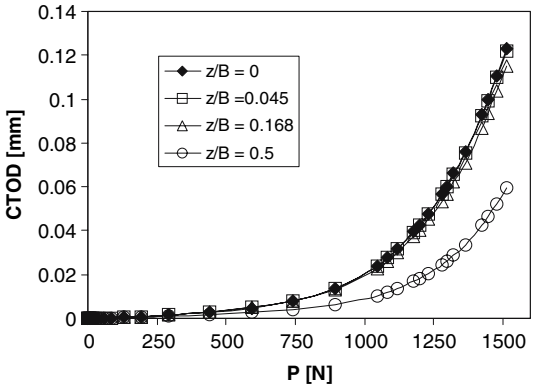

Fig. 8 Crack-tip opening displacement (CTOD) versus applied load

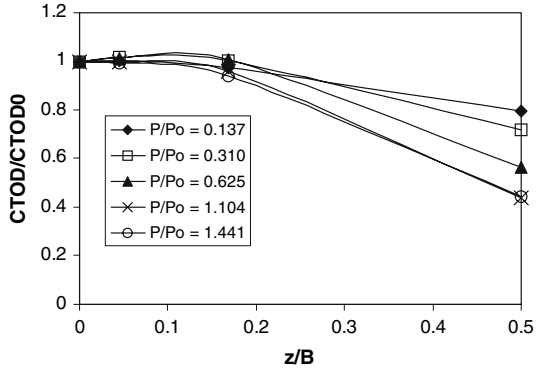

Fig. 9 Crack-tip opening displacement (CTOD) versus applied load for various load ratios P/P_0

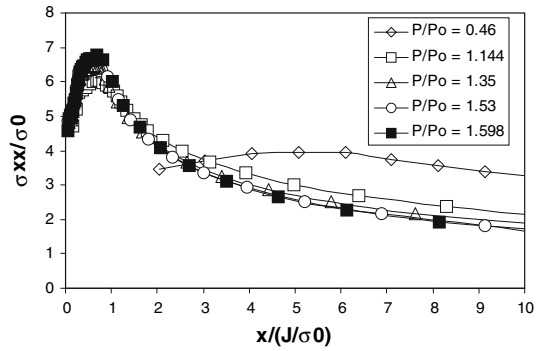

Fig. 10 Stress normalized versus normalized crack-tip distance

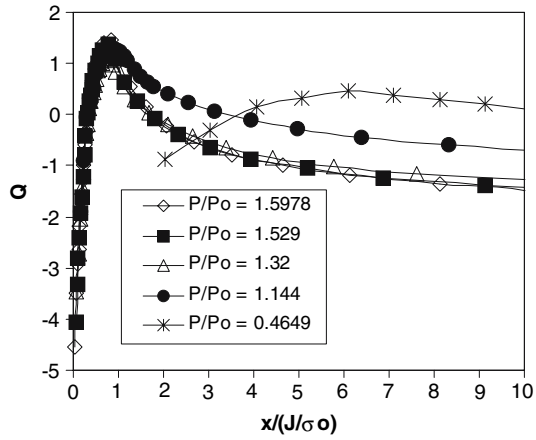

Fig. 11 *Q* triaxiality factor versus normalized crack-tip distance

Fig. 10, for different load levels ratio ranging from contained yielding (P/P_0 = 0.46) to large-scale plasticity (P/P_0 = 1.6). A normalizing factor J/σ_o for the crack-tip distance is convenient to use because the blunted crack opening is given roughly by J/σ_0. This value sets the local size scale on which large strains and stresses develop and the microscopic ductile fracture processes occurs.

The full-field finite element results around the crack-tip together with the HRR asymptotic field results, gives the triaxiality factor *Q* according to relation (4). Results of *Q* values versus crack-tip distance normalized by J/σ_0 is shown in Fig. 11 for a wide range of applied load ratios, from contained plasticity (P/P_0 = 0.46) to a large yield condition (P/P_0 = 1.6).

The *Q* triaxiality parameter shows in the range of $2 < r/(J/\sigma_0) < 7$ a small dependence on *r*, only up to loads of P/P_0 = 0.46, as it has been reported by other investigators. However, as far as the load ratio increase over the value of P/P_0 = 0.46, the *Q* factor starts to deviate from the previous steady value in the region defined by $r < 4(J/\sigma_0)$. At higher load levels, the plastic zone develops a progressive compressive stress region, starting from the free boundary and gradually extended to the crack-tip region. For the very near-crack-tip region, $r < 1(J/\sigma_0)$, there is a drastic breakdown in the *Q*

behavior. This phenomenon is consistent with the existence of large nonlinear effects on that region invalidating the HRR asymptotic stress field based upon small strain theory.

5. Summary and Conclusions

Failure assessment of the integrity of a flawed structure has been based on the dominance of asymptotically singular crack-tip field, characterized by a single parameter, such as the *J*-integral. The *J*-integral parameter measures the intensity of the crack-tip stress/deformation fields around the crack-tip and has proven to be a viable parameter for predicting ductile crack initiation and growth under monotonic loading. However, for specimens with a low crack-tip constraint, the dominance of single-parameter based singular fields exists only at small plasticity. At large plasticity, the crack-tip triaxiality of low-constraint specimens is lower than the predicted by the single-parameter based singular fields. Consequently, such specimens often exhibit higher fracture toughness than high-constraint specimens if the fracture process occurs after large plastic deformation. This behavior is referred to as constraint effects in fracture.

Constraint effects in fracture are closely related to the crack-tip behavior, which is complex because the fracture process zone occurs close to the crack-tip where finite strain and high gradient stress/strain exist. Moreover, a finite deformation blunting of the crack-tip exists and hence, small strain theory does not model blunting correctly. Strain gradients that develop around a crack front cause deformation in the local region to be constrained by the surrounding material. The level of constraint depends upon the crack configuration and crack location relative to external boundaries. Finally, constraint effects produce a three-dimensional crack-tip stress field, which differs from those in plane strain and plane stress, and strongly influence fracture behavior. Therefore, for a clear understanding of the three-dimensional crack-tip field behavior, a full and detailed three-dimensional finite element analysis needs to be performed.

In this paper, an accurate and detailed numerical solution of the asymptotic crack-tip stress field was obtained for a deep crack in a three-point bend specimen, for an applied load ranging from contained plasticity ($P/P_0 = 0.46$) to a fully plastic condition ($P/P_0 = 1.6$). Crack-tip blunting, occurring at the crack-tip as the load is increasing, was modeled with a small notch radius at the tip crack.

Numerical results of the stress crack-tip field were used to evaluate a second fracture mechanics parameter Q, which conveys the notion of a triaxiality stress condition and is used as a constraint measure of the crack-tip. A negative value of Q implies that a low constraint occurs in the cracked structural component, in such a way that the single one parameter *J*-approach does not represent adequately the asymptotic crack-tip stress field.

The average *J*-integral values and CTOD exhibit a notable variation along the crack front with increasing plastic deformation. This supports the necessary requirement to use a three-dimensional crack-tip analysis in the specimen.

When the applied load produces a moderate yield condition in the ligament, typically $P/P_0 = 0.46$ in our specimen, the *J*-Q approach represents a good alternative to evaluate the structural integrity of a three-dimensional cracked structural component. However, when medium to large yield scale conditions is attained, the Q triaxiality parameter is markedly dependent of the position on the fracture process zone. Hence, the *J*-Q methodology is invalidated, because the assumed Q independence of the spatial coordinates in the near-crack-tip is not fulfilled.

Acknowledgments

The author acknowledges the financial support of FONDECYT-CHILE and the Universidad Técnica Federico Santa Maria, Research Project DGIP 25.06.22.

References

1. J.W. Hutchinson, Singular Behavior at the End of a Tensile Crack in a Hardening Material, *J. Mech. Phys. Solids*, 1968, **16**, p 13–31
2. J.R. Rice and G.F. Rosengren, Plane Strain Deformation Near a Crack Tip in a Power Law Material, *J. Mech. Phys. Solids*, 1968, **16**, p 1–12
3. J.A. Begley and J.D. Landes, The Integral *J* as a Fracture Criterion, *Fracture Toughness*, ASTM STP-514, 1972, p 1–23
4. J.W. Hutchinson, Fundamentals of the Phenomenological Theory of Nonlinear Fracture Mechanics, *J. Appl. Mech.*, 1983, **50**, p 1042–1051
5. J.D. Sumpter, An Experimental Investigation of the T Stress Approach, *Constraint Effects in Fracture*, ASTM STP 11171, E.M. Hackett, K.H. Schwalbe, and R.H. Dodds, Ed., American Society for Testing and Materials, 1995, p 43–67
6. ASTM Standard Test Method for Measurement of Fracture Toughness, ASTM E 1820-99, *ASTM Annual Book of Standards*, Vol 03.o1, 1999
7. J.D. Landes, Elastic-Plastic Fracture Mechanics: Where has it been? Where is it Going, *Fatigue and Fracture Mechanics*, Vol 30, ASTM STP 1360, P.C. Paris, K.L. Jerina, Ed., 1999, p 3–18
8. N.P. O'Dowd and C.F. Shih, Family of Crack-Tip Fields Characterized by a Triaxiality Parameter. I. Structure of Fields, *J. Mech. Phys. Solids*, 1991, **39**, p 898–1015
9. N.P. O'Dowd and C.F. Shih, Family of Crack-Tip Fields Characterized by a Triaxiality Parameter. II. Fracture Applications, *J. Mech. Phys. Solids*, 1992, **40**, p 939–963
10. C. Betegon and J.W. Hancock, Two-Parameter Characterization of Elastic-Plastic Crack-Tip Fields, *J. Appl. Mech.*, 1991, **68**, p 104–110
11. J.W. Hancock, W.G. Reuter, and D.M. Parks, Constraint and Toughness Parameterized by T, *Constraint Effects in Fracture*, ASTM STP 1171, E.M. Hackett, Ed., American Society for Testing and Materials, 1993, p 21–40
12. R.H. Dodds, C. Ruggieri, and K. Koppenhoefer, 3-D Constraint Effects on Models for Tranferability of Cleavage Fracture Toughness, *Fatigue and Fracture Mechanics*, Vol 28, ASTM STP 1321, J.H. Underwood, B.D. MacDonald, and M.R. Mitchell, American Society for Testing and Materials, 1997, p 179–197
13. Y.Y. Wang and D.M. Parks, Limits of *J-T* Characterization of Elastic-Plastic Crack-Tip Fields, *Constraint Effects in Fracture*, ASTM STP 1244, M. Kirk and A. Bakker, Ed., American Society for Testing and Materials, 1995, p 43–67
14. C.F. Shih, Relationship Between the *J*-Integral and the Crack Opening Displacement for Stationary and Extending Cracks, *J. Mech. Phys. Solids*, 1981, **29**, p 305–326